Journal homepage: http://gwse.iheg.org.cn

Original Article

Groundwater recharge via precipitation in the Badain Jaran Desert, China

Zhe Wang[1,2], Li-juan Wang[1,2*], Jian-mei Shen[1], Zhen-long Nie[1], Le Cao[1], Ling-qun Meng[1,2]

[1] *Institute of Hydrogeology and Environmental Geology*, *Chinese Academy of Geological Sciences*, *Shijiazhuang* 050061, *China*.
[2] *Technology Innovation Center for Geothermal & Hot Dry Rock Exploration and Development*, *Ministry of Natural Resources*, *Shijiazhuang* 050061, *China*.

Abstract: Precipitation infiltration serves as a significant source of groundwater in the Badain Jaran Desert. To investigate variations in precipitation infiltration within the desert, this study collected data on moisture content and temperature from the vadose zone through in-situ field monitoring. Utilizing these data, a numerical model is employed to explore the mechanism of groundwater recharge via precipitation. The results are as follows: (1) Moisture content and temperature in the shallow vadose zone exhibit significant seasonal variations, with moisture content diminishing with increasing depth; (2) Groundwater recharge via precipitation infiltration initially increases and then decreases with groundwater level depth (GWD). Peak groundwater recharge via precipitation occurs at a GWD of 0.75 m, decreasing to merely 0.012 cm at GWDs exceeding 2 m; (3) Groundwater is no longer susceptible to phreatic water evaporation when the GWD reaches approximately 3.7 m. Therefore, GWD plays a crucial role in governing groundwater recharge via precipitation in the Badain Jaran Desert.

Keywords: Badain Jaran Desert; Vadose zone; Groundwater recharge; In situ monitoring; Numerical simulation

Received: 25 Apr 2023/ Accepted: 26 Nov 2023/ Published: 15 Mar 2024

Introduction

Deserts exhibit vulnerable ecological environments, with evaporation rates exceeding precipitation levels. Moisture plays a crucial role in influencing the growth of herbaceous plants and the movement of dunes within desert landscapes (Liu et al. 2015; Zhong, 2016). Hence, precipitation holds significant importance in the ecological water cycle of deserts. The Badain Jaran Desert, known for its diverse landforms and the coexistence of lakes and megadunes, has attracted considerable attention. It manifests low moisture content in the vadose zone, posing challenges for accurately calibrating hydrogeological parameters. Conventional research methods for groundwater recharge are often inadequate for desert environments (Liu et al. 2010), leading to increased academic interest in understanding the impact of rainfall on desert ecosystems. Numerous scholars have investigated precipitation and water cycle in the Badain Jaran Desert. Zhang et al. (2020) utilized remote sensing imagery to calculate regional phreatic water evaporation using groundwater dynamic information and a phreatic water evaporation model, contributing to the assessment of water balance in the desert. Ning et al. (2021) and Zhang et al. (2023) analyzed spatio-temporal changes in soil moisture content, precipitation, and temperature, providing valuable insights into the hydrographic characteristics of the desert. Cao et al. (2021) utilized stable isotopes as natural tracers to investigate the source of water vapor for precipitation in the desert. They concluded that water vapor for intra-annual precipitation primarily origi-

*Corresponding author: Li-juan Wang, *E-mail address*: 32737195@qq.com

DOI: 10.26599/JGSE.2024.9280009

Wang Z, Wang LJ, Shen JM, et al. 2024. Groundwater recharge via precipitation in the Badain Jaran Desert, China. Journal of Groundwater Science and Engineering, 12(1): 109-118.

nates from westerly wind masses, with contributions from both spring and summer monsoons in the southeastern desert. Utilizing hydrogeochemical zoning pattern and stable isotopes of hydrogen and oxygen, Wei et al. (2019) explored the groundwater recharge mechanism in the water source area on the southern margin of the desert, and revealed significant groundwater recharge from pulsed rivers formed by precipitation in certain areas.

The Badain Jaran Desert is characterized by large GWDs, uniform lithologies, and high permeabilities in the vadose zone. Given the significance of precipitation as a primary groundwater recharge source in the desert, it becomes crucial to quantitatively assess groundwater recharge via precipitation. This study addresses this need by conducting in-situ tests to monitor moisture content and temperature along the vadose zone profile, combined with numerical simulation methods. A water-vapor-heat migration model for the desert's vadose zone is constructed by analyzing variations in moisture content and temperature. Through this model, the study quantitatively revealed the process of groundwater recharge via precipitation and accurately estimated the recharge intensity, thus providing a scientific foundation for precisely calculating regional groundwater resources. The findings of this research hold both theoretical significance and practical value, offering insights for the rational production and utilization of groundwater resources as well as ecological protection in the Badain Jaran Desert.

1 Study area

The Badain Jaran Desert spans approximately 354 km in the N-S direction (39°30′N–41°38′N) and about 442 km in the E-W direction (99°48′E–104°14′E), covering an area of 50,000 km^2, making it the third largest desert in China (Zhang et al. 2022). Positioned south of the Guaizi Lake, east of the Gurinai Lake, north of the Beida Mountain, and west of the Yabulai and Zongnai mountains, its reach extends northward to the south of the Ejina Plain and eastward to the Tamusu area, connecting with the Tengger Desert in the east of Alxa (Xiao et al. 2023). The desert's terrain features higher elevations in the south and lower elevations in the north, with significant local topographic variations due to megadunes (Jiang et al. 2022; Zhang et al. 2022). It experiences a temperate continental desert steppe climate, characterized by sparse rainfall, aridity, frequent sandstorms, extremely hot summers, and significant diurnal temperature variations. Annual precipitation averages between 80–120 mm, while annual evaporation exceeds 3,000 mm. Surface runoff is barely observed due to extensive evaporation, resulting in large GWDs. Vegetation in the desert includes trees, shrubs, herbs, reeds, and achnatherum splendens, along with windbreak and sand-fixing species such as Haloxylon ammodendron, Caragana korshinskii, Zygophyllum xanthoxylum, Artemisia sphaerocephala, Populus euphratica, and Alhagi camelorum.

This study conducted in-situ field tests on the Badain Lake, situated on the southern margin of the Badain Jaran Desert. The lake area is dominated by barchan dunes and dune chains in the southeast, gradually transitioning into pyramidal megadunes and tall composite sand mountain in the northwest (Fig. 1). The Badain Lake area predominantly consists of typical splayed lakes, with ridge lines generally extending northeastward at 30°–50° angles, dividing the lake into eastern and western sections.

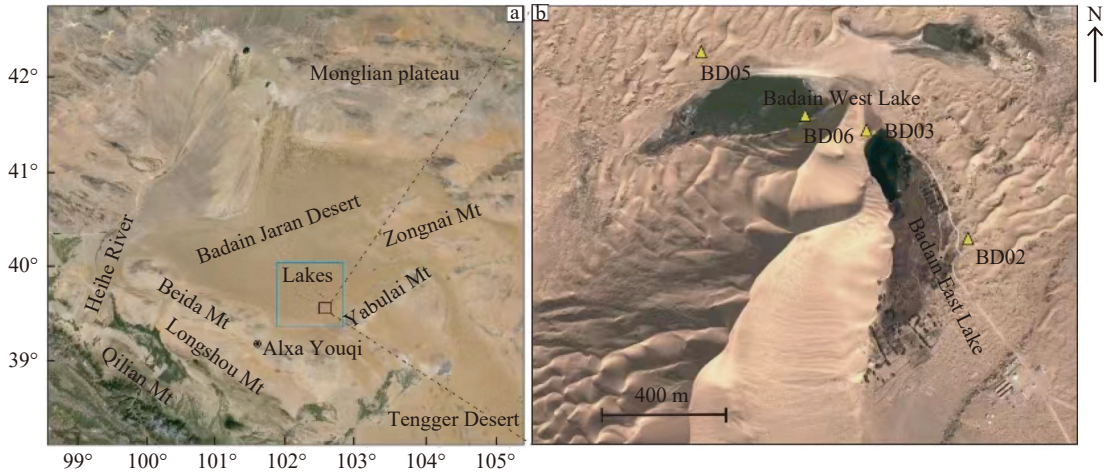

Fig. 1 Location maps of the Badain Lake test sites

2 Study methods

2.1 In situ field tests

To obtain data on moisture content and temperature in the vadose zone at the test sites, this study deployed monitoring instruments in the lake area for long-term observation. Fig. 1 shows two observation sites, positioned 15 m and 50 m southeast of Badain Lake, respectively. These sites correspond to GWDs of approximately 2.5 m and 4.8–5 m.

The moisture content and temperature data from German A755 STMP monitoring instruments were transmitted to the Advantage Pro platform. These were deployed at specific burial depths, as illustrated in Fig. 2. At site A, the burial depths for both moisture content and temperature sensors were 0.1 m, 0.3 m, 0.5 m, 1.2 m, 2.0 m, 0.2 m, 0.4 m, 1.0 m, 1.8 m, and 2.6 m. At site B, the burial depths were 0.1 m, 0.3 m, 0.5 m, 0.8 m, 1.2 m, 1.6 m, 2.4 m, 2.8 m, 3.2 m, and 4.2 m. The observational frequency for both sites was set at 1 h per time interval. Additionally, meteorological data were obtained through real-time monitoring by a small automatic meteorological station installed at Badain Lake. The observational frequency for this station was set at 0.5 hour per time interval.

2.2 Numerical model construction

2.2.1 Model principle

This study employed Hydras-1D software to construct a one-dimensional unsaturated soil water-heat migration model, simulating the mechanism of groundwater recharge via water infiltration in the vadose zone. The incorporation of meteorological conditions helped mitigate the usage limitations of the software (Yang et al. 2021; Zhang et al. 2021). Additionally, parametric inversion was conducted using various soil parameter databases within the software to obtain optimal hydrogeologic parameters (Wang, 2015).

The model considered the coupled water-vapor-heat migration in soil, with its governing equation expressed as follows:

$$\frac{\partial \theta}{\partial t} = -\frac{\partial q_L}{\partial z} - \frac{\partial q_v}{\partial z} - S \tag{1}$$

Where: q_L and q_v denote the volumetric flux of liquid and vapourous water, respectively, in cm/d; t indicates time in days; z represents vertical coordinate axis with positive values upwards, in cm, and S stands for the source-sink term accounting for soil moisture for plant roots. Since root water uptake was not involved in the tests due to the absence of plants, S was excluded (taken as 0).

The model also incorporated the following equations:

$$\theta(h) = \theta_r + \frac{\theta_s - \theta_r}{[1 + |\alpha h|^n]^m} \quad h < 0 \tag{2}$$

$$K(h) = K_s S_e^i [1 - (1 - S_e^{1/m})^2]^2 \quad h < 0 \tag{3}$$

$$S_e = \frac{\theta - \theta_r}{\theta_s - \theta_r} \tag{4}$$

Where: S_e denotes the effective moisture con-

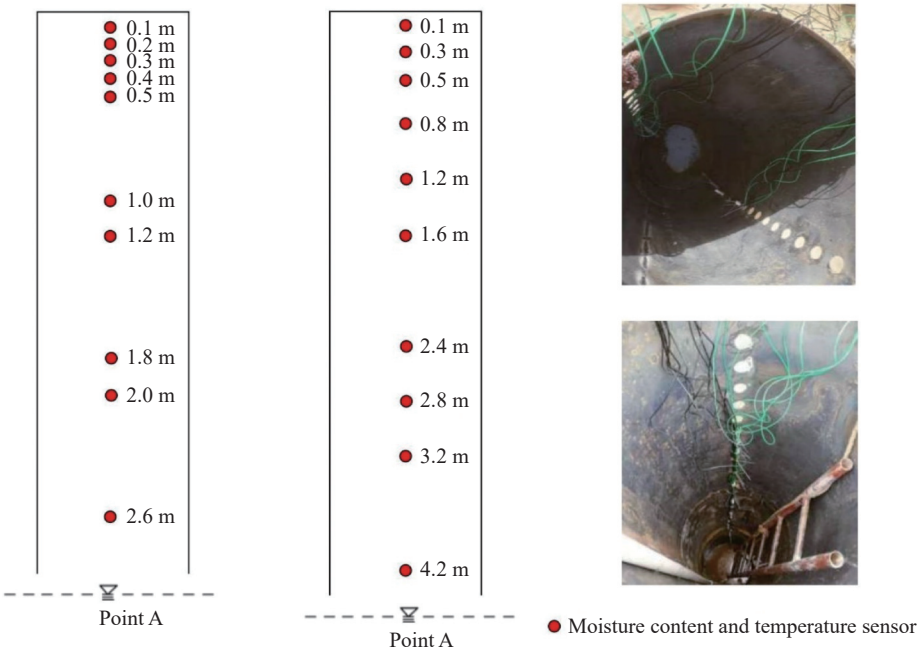

Fig. 2 In situ observation profiles

tent, dimensionless; θ represents the soil volumetric moisture content, cm^3/cm^3; θ_r stands for the residual moisture content, cm^3/cm^3; θ_s indicates the saturated moisture content, cm^3/cm^3; K_s means the saturated permeability coefficient, cm/d; α, n, and m represent the shape parameters of the model, $m = 1 - 1/n$, and l is the gap connectivity parameter, generally taken as 0.5.

2.2.2 Model construction and parameter input

For moisture migration modeling, the Van-Genuchten model was selected as the soil hydraulic model, with the atmospheric boundary serving as the upper boundary and meteorological conditions as the non-stable boundaries. Due to the considerable thickness of the vadose zone in the study area, the free-drainage boundary was selected as the lower boundary for calculation. The simulated soil thickness was 300 cm at site A and 600 cm at site B. Based on experimental results from soil particle analysis, the soil texture along the profile depth of the study area was determined to be fine sand. The observation period lasted from April 1, 2019 to May 14, 2019, totaling 44 days, with each day representing a time step. The initial moisture content and temperature of the vadose zone on April 1, 2019, were used as the initial values in the simulation (Figs. 4 and 6). Meteorological data for the simulation period are shown in Table 1.

2.2.3 Model precision validation

To ensure the accuracy and precision of the model, this study conducted validation of the simulation results. Initially, analytical tests were carried out on various hydraulic parameters (Fig. 5-1). Subsequently, precision validation was performed using root mean square error (RMSE), relative error (RE), and Nash-sutcliffe efficiency coefficient (NSE). The calculation equations for these evaluation indices are as follows (Nash and Sutcliffe,

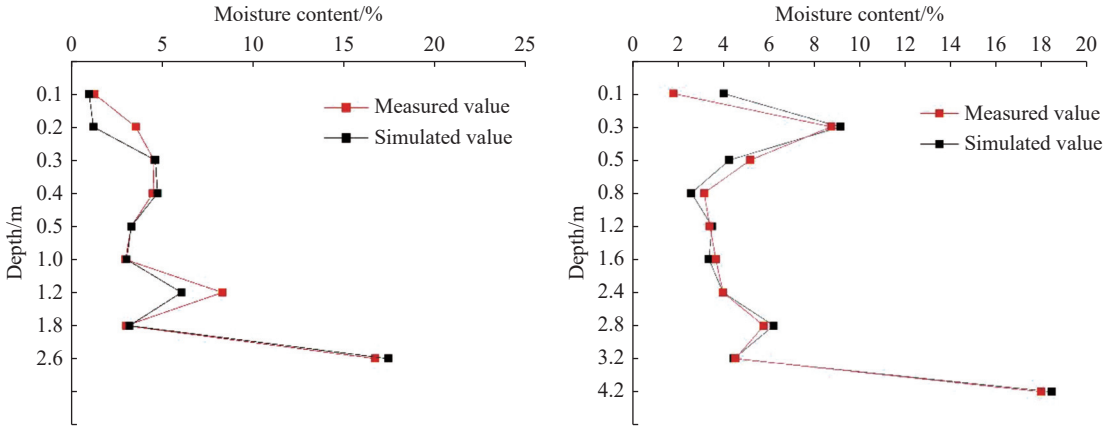

Fig. 3 Comparison between simulated and measured moisture content values of soil profiles at sites A and B

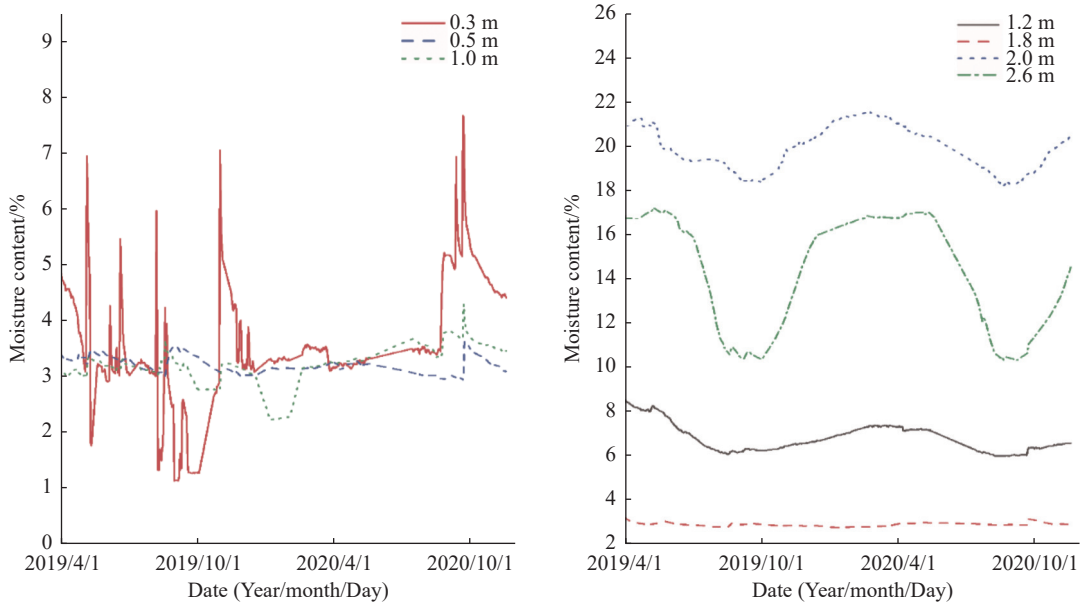

Fig. 4 Variations in the moisture content of the soil profile at site A

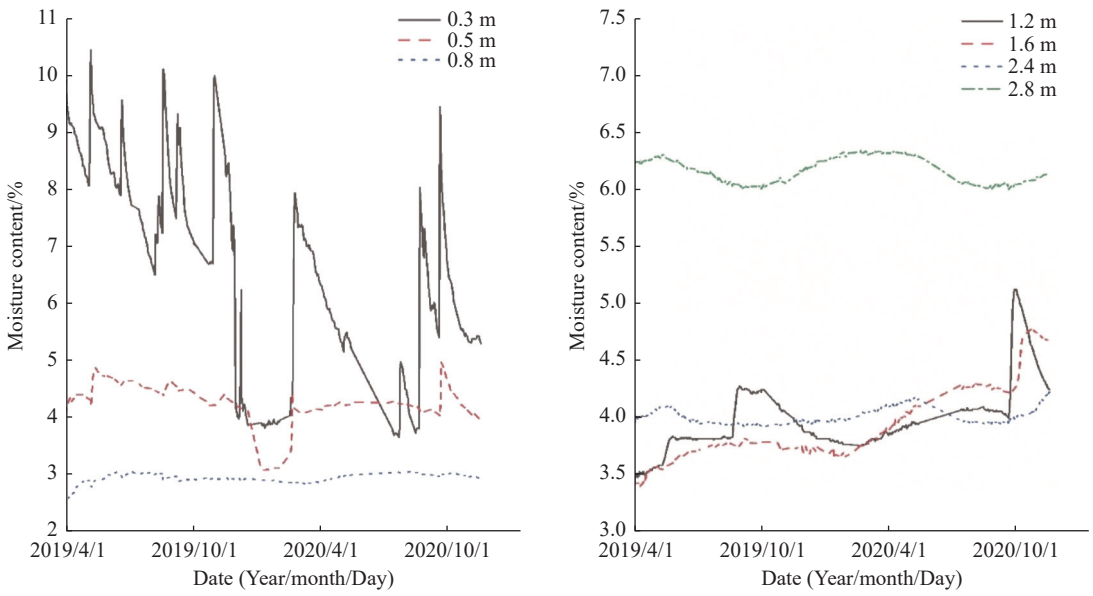

Fig. 5 Moisture content at different depths of site B

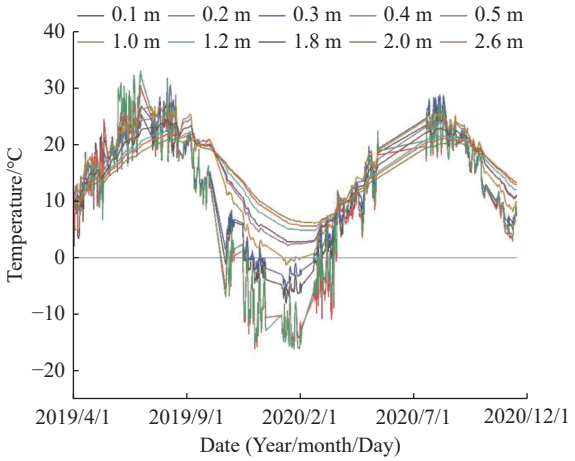

Fig. 6 Variations in soil temperature at different depths of site A

1970):

$$RMSE = \sqrt{\frac{1}{N}\sum_{i=1}^{N}(S_i - O_i)^2} \quad (5)$$

$$RE = 1 - \frac{\sum_{i=1}^{N}(S_i - O_i)^2}{\sum_{i=1}^{N}\left(S_i - \bar{O}\right)^2} \quad (6)$$

$$NSE = 1 - \frac{\sum_{i=1}^{N}(S_i - O_i)^2}{\sum_{i=1}^{N}\left(O_i - \bar{O}\right)^2} \quad (7)$$

Where: S_i denotes the simulated value for the sample i; O_i represents the measured value for the sample i; $\bar{O}$ signifies the average of measured values, and N indicates the sample size. Among the above three evaluation indices, *RMSE* represents the degree of dispersion, *RE* shows the confidence level of a simulated value, and *NSE* means the coincidence level between simulated and measured values over time. Generally, a simulated value is acceptable in the case of NSE> 0.5.

2.3 Model identification and validation

Through continuous fine-tuning of parameters based on preliminary fitting results and expected outcomes, efforts were made to achieve maximum proximity between simulated and measured values, thereby minimizing errors. Furthermore, comparison diagrams illustrating simulated and measured soil moisture content values were plotted based on the fitting results, as shown below:

Fig. 3 compares the variation trends in soil moisture content at sites A and B using simulated and measured profiles. The simulated and measured values at site A show high consistency, with a maximum difference below 0.35%, suggesting a strong overall fitting degree. Similarly, the comparison revealed a high degree of fitting for soil

Table 1 Meteorological data for the simulation period (cm)

Date	Precipitation	Date	Precipitation	Date	Precipitation
4.8	2.6162	5.5	2.6162	5.8	0.2032
4.24	0.2032	5.6	6.4516	5.9	0.6096
4.28	0.4064	5.7	8.3312	5.10	0.4064

moisture ate site B between simulated and measured values. Model precision errors, as assessed by RMSE, RE, and NSE are presented in Table 2. The calculation results affirm that the model and various soil hydraulic parameters are fully applicable for investigating moisture migration in the vadose zone of the study area.

3 Results and analysis

3.1 Variations in the moisture content of the vadose zone

To gain further insight into the formation mechanism of the stable infiltration zone of water in the vadose zone, this study investigated the variations in water content in the vadose zone at different depths, elucidating the seasonal dynamics of moisture content. The moisture content of the vadose zone and the corresponding meteorological data for sites A and B during the observation period are shown in Figs. 4 and 5.

Fig. 4 reveals the following findings. (1) Moisture content at a depth of 0.3 m experiences drastic changes due to precipitation. It typically rises sharply after precipitation, reaching a peak, and then gradually decreases as the soil dries out. The magnitude of variations diminishes with increasing depth. (2) In contrast, moisture content at depths of 0.5 m and 1 m exhibits minor variations, with increased values in winter and decreased values in summer. These depths experience short-term effects from seasonal freeze-thaw and show a nonsignificant response to precipitation, with only a slight increase in moisture content, which roughly ranges from 3% to 4%; (3) Variations in moisture content decrease with depth. Deeper burial depth corresponds to smaller and more stable variations in moisture content.

Fig. 5 illustrates the following results: (1) Moisture content at a depth of 0.3 m closely correlates with precipitation, rising sharply after rainfall events and gradually decreasing thereafter; (2) Moisture content in the shallow vadose zone decreases to some extent during winter when the temperature falls below 0°C, likely due to moisture freezing. As temperature rises above 0°C in spring, frozen water gradually thaws, leading to increased moisture content; (3) The moisture content at a burial depth of 0.5 m exhibits subtle variations, with increased values in summer and decreased values in winter, influenced by seasonal freeze-thaw cycles; (4) Moisture content at a burial depth of 1.0 m remains relatively stable at around 3%, unaffected by the seasonal freeze-thaw cycles.

Overall, the moisture content data for different depths of sites A and B, along with corresponding meteorological data, indicate that moisture content at varying depths is influenced by precipitation, especially at a depth of 30 cm. During the continuous precipitation events, moisture content at a depth of 30 cm rises sharply, but quickly returns to normal levels afterward. In contrast, moisture content at depths of 50 cm and 100 cm exhibits slower responses to precipitation and smaller variation ranges. This can be attributed to the prolonged arid conditions of the vadose zone, resulting in less precipitation and lower precipitation intensity. As a result, most of the moisture is retained in the shallow soil. Consequently, while moisture content at a depth of 30 cm rapidly increases with precipitation, whereas that at depths of 50 cm and 100 cm undergoes only minor variations following precipitation. Increasing depth corresponds to more retained water and a longer response times of moisture content to precipitation. Ultimately, precipitation ceases to significantly influence the moisture content when the depth reaches a certain extent.

3.2 Variations in the temperature of the vadose zone

3.2.1 Seasonal variations in the temperature of the vadose zone

Seasonal variations in the temperature of the vad-

Table 2 Error verification of soil moisture content at different burial depths of sites A and B

	Observation location/m	RMSE/$cm^3 \cdot cm^3$	RE/%	NSE
Site A	0.3	0.00608	1.88042	0.85371
	0.5	0.00153	0.83435	0.74795
	1.0	0.00171	0.79379	0.56166
Site B	0.3	0.00683	1.28142	0.71449
	0.5	0.00357	0.77259	0.63852
	1.2	0.00121	0.69508	0.57253
	2.4	0.00118	0.63225	0.56166

ose zone depict temporal patterns of temperature across different seasons of a hydrological year. The temporal variations in temperature at various depths, as plotted in Fig. 6, reflect response times to meteorological conditions during the same period.

Fig. 6 illustrates temporal variation patterns of temperature at depths of site A from April 2019 to November 2020. The variations in the temperature of the vadose zone are primarily influenced by atmospheric temperature. As depth increases, temperature in the vadose zone gradually decreases. Heat absorbed by the topsoil is transmitted downwards, elevating the temperature of deeper soil. The soil temperature within the entire vadose zone profile is influenced by atmospheric temperature, the effect of which weakens significantly with a certain delay as the soil depth increases. Soil temperature displays the most significant and largest variations near the surface, gradually stabilizing with increasing depth.

3.2.2 Depth-based variations in soil temperature

The Badain Jaran Desert experiences significant diurnal temperature fluctuations, leading to rapid temperature changes in sandy soil, a typical characteristic of soil temperature in the study area. In addition to gravity, temperature gradients also have a significant influence on moisture migration in the vadose zone. Therefore, it is essential to investigate the variation curves of soil temperature along the profile.

Fig. 7 illustrates the temperature variations of soil in the vadose zone at different depths of site A. As the depth increases, the temperature variation range gradually narrows, ranging, for instance, from −16–32°C on the surface to 4–2°C at a depth of 2.6 m. Additionally, there is a significant attenuation trend in the intra-annual seasonal variation range. Drastic seasonal variations of soil temperature within a depth of 0.5 m suggest that temperature in the shallow soil is significantly influenced by atmospheric temperatures in different seasons. Increasing depth is associated with a narrowing intra-annual variation range of soil temperature, and soil temperature at the same depth exhibits relatively gentle intra-annual seasonal variations. This indicates that as depth increases, soil temperature demonstrates a smaller seasonal variation range and gentler variations.

3.3 Simulation of soil moisture migration at different GWDs of the vadose zone

The Badain Jaran Desert experiences a typical extremely arid continental climate, characterized by intense evaporation and scarce precipitation, with annual evaporation exceeding 3,000 mm and precipitation below 200 mm. Despite this, over 100 lakes spread across the desert. Hence, further exp-

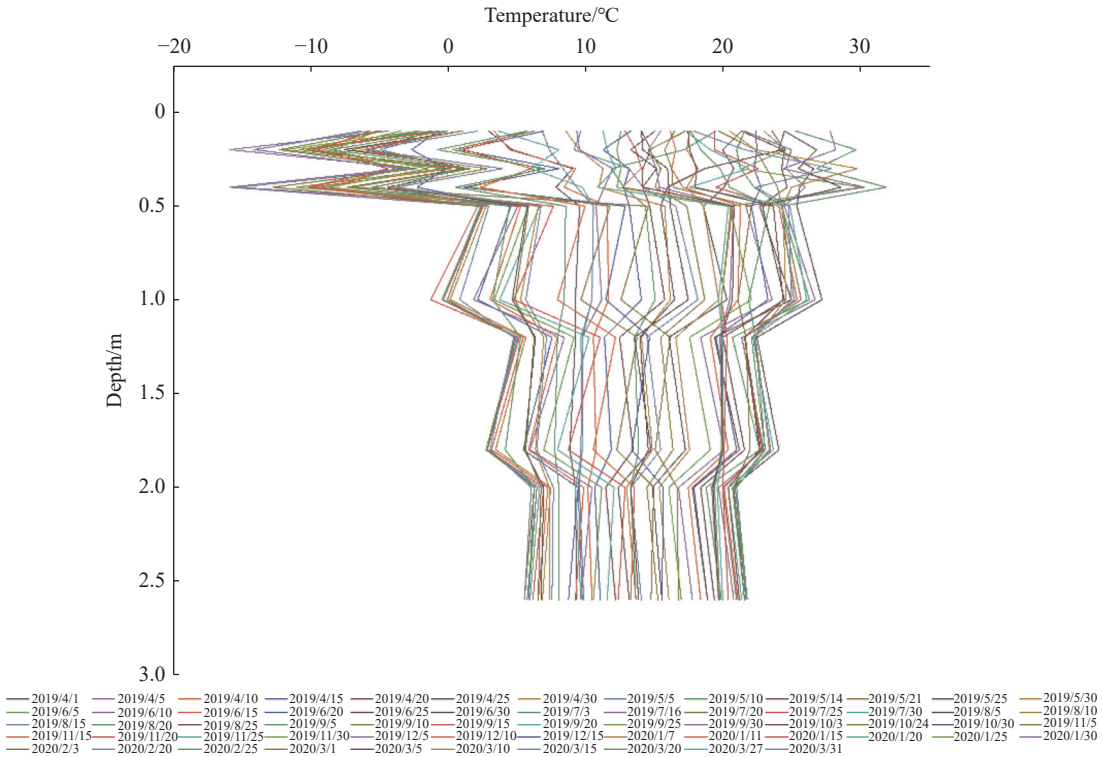

Fig. 7 Variations in soil temperature at different depths of site A

loration of the moisture migration mechanism of the vadose zone is critical for identifying the source and recharge mechanism of groundwater in the desert.

Using various GWDs set with the Hydrus-1d software, this study investigated the influence patterns of GWDs on groundwater recharge via precipitation infiltration. Accordingly, relationships between GWD and groundwater infiltration and between GWD and groundwater evaporation, were plotted, as shown in Figs. 8 and 9.

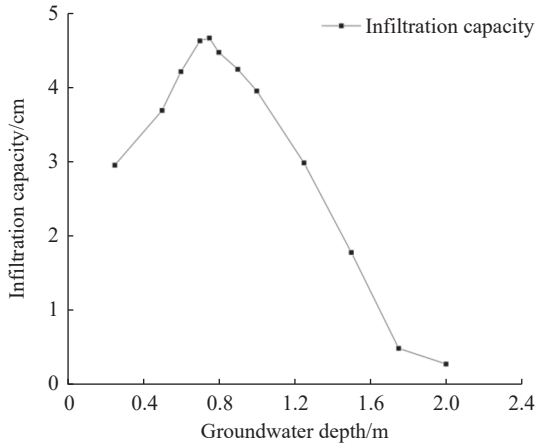

Fig. 8 Relationship between groundwater level depths and groundwater infiltration

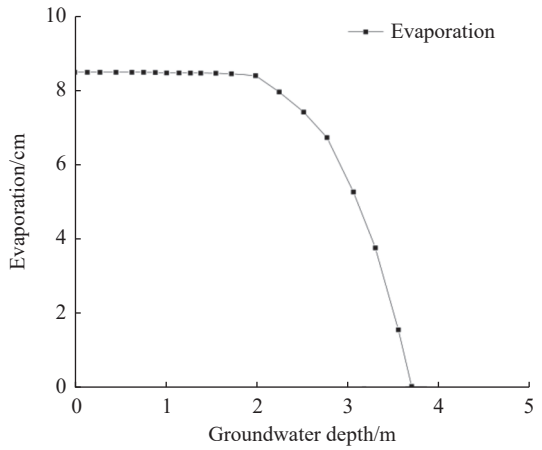

Fig. 9 Relationship between groundwater level depths and evaporation

As illustrated in Fig. 8, as the GWD increases, groundwater recharge from atmospheric precipitation infiltration initially rises continuously, reaching a peak value of 4.6576 cm at a burial depth of approximately 0.75 m. After reaching this peak, it gradually declines. This trend can be explained as follows: Shallow GWDs allow for relatively high moisture content in the shallow vadose zone, facilitating smooth groundwater recharge by precipitation, with any excess forming surface runoff. With increasing burial depth, the vadose zone can accommodate more water, leading to a concurrent increase in groundwater recharge. However, after reaching the recharge peak, the increasing thickness of the vadose zone hampers water infiltration despite more water in the zone. Eventually, at a certain depth, no groundwater recharge occurs as all precipitation is retained in the vadose zone.

Fig. 9 illustrates that evaporation from the phreatic surface decreases gradually with increasing GWD. Shallow GWDs result in strong and significant groundwater evaporation. As depth increases, the vadose zone thickens and accumulates more capillary water, leading to a sharp decline in groundwater evaporation. Moreover, the influence of atmospheric evaporation on groundwater diminishes as depth increases, with no groundwater evaporation observed at a depth of approximately 3.7 m.

4 Conclusions

The Badain Jaran Desert experiences an arid climate, with precipitation lower than evaporation. Despite this, it boasts over 100 lakes, including some freshwater lakes. To identify the source of groundwater in the desert and understand the moisture migration patterns of its vadose zone, this study conducted in-situ precipitation infiltration tests in the desert. Based on the obtained test data, the findings of this study can be summarized as follows:

(1) Moisture content generally exhibits low values in shallow layers and high values in deep layers. In terms of overall seasonal variations, shallow moisture content varies significantly with seasons, whereas deep moisture content shows minor variations. Both moisture content and soil temperature vary dramatically in the shallow vadose zone.

(2) The moisture migration model for the vadose zone, established using the Hydrus-1d software, demonstrates highly consistent variations between simulated and measured results, accurately representing the actual situation. Precision verification results indicate that the evaluation coefficients of both simulated values and verified results fall within the required range, with NSE over 0.5, meeting precision requirement. Therefore, the model is applicable for investigating moisture migration patterns in the vadose zone of the study area.

(3) Groundwater recharge via precipitation infiltration increases and then decreases with GWD,

reaching its maximum at a GWD of 0.75 m. Groundwater evaporation decreases sharply and then gradually with increasing GWD. Groundwater is free from evaporation influence when GWD reaches approximately 3.7 m, with no phreatic water evaporation.

Acknowledgements

This work was funded by China Geological Survey Program (121201106000150093).

References

Cao L, Shen JM, Nie ZL, et al. 2021. Stable isotopic characteristics of precipitation and moisture recycling in Badain Jaran Desert. Earth Science, 8: 2973−2983.

Jiang GL, Wang NA, Li ZL, et al. 2022. Distribution pattern of saline minerals in surface sediments from lakes in the Badain Jaran desert and its implications for climate-environmental reconstruction. Geology in China. (in Chinese) https://kns.cnki.net/kcms/detail/11.1167.P.20220524.1358.002.html

Liu H, Zhou HF, Liu X. 2015. Analysis of soil moisture migration on sand dune under the condition of heavy rain-fall. Journal of Soil and Water Conservation, 2: 157−182. (in Chinese) DOI：10.13870/j.cnki.stbcxb.2015.02.02.

Liu XY, Chen JS, Sun XX. 2010. Application of chloride tracer method to study replenishment ratio of precipitation in desert. Transactions of the CSAE, 1: 146−149. DOI：10.3969/j.issn.1002-6819.2010.z1.028.

Nash JE, Sutcliffe JV. 1970. River flow forecasting through conceptual models part I-A discussion of principles. Journal of Hydrology, 3: 282−290. DOI：10.1016/0022-1694(70)90255-6.

Ning WX , Liu XY, Wang ZT. 2021. Temperature and precipitation characteristics and spatial stratified heterogeneity in Badain Jaran Desert. Journal of University of Chinese Academy of Sciences, 1: 103−113. DOI：10.7523/j.issn.2095-6134.2021.01.013.

Wang B. 2015. Research on the water transport law of the aerated zone in the Zhongning Plain based on hydras-1D. M. S . thesis. China University of Geosciences (Beijing): 20−30.

Wei SB, Nie ZL, Shen JM, et al. 2019. Research on groundwater recharge mechanism in the South Fringe of Badain Jaran Desert. Yellow River, 2: 88−93. (in Chinese) DOI：10.3969/j.issn.1000-1379.2019.02.018.

Xiao YT, Zhang GM, Hong C , et al. 2023. Sand-dust horizontal flux of different surfaces in the western margin of Badain Jaran Desert. Journal of desert research, 2: 104−113. DOI：10.7522/j.issn.1000-694X.2022.00110.

Yang F , He YP, Hong DL, et al. 2021. Effect of controlled irrigation and drainage on the capillary rise in Paddy Fields simulated using the HYDRUS-1D Model. Journal of Irrigation and Drainage, 11: 90−97. (in Chinese) DOI：10.13522/j.cnki.ggps.2021225.

Zhang JH , Niu ZM, Ma SG, et al. 2023. Water characteristics and hydrological significance of Tamarix laxa distribution in the Mega Dune of Badain Jaran Desert. Journal of Capital Normal University (Natural Science Edition), 2: 53−59. (in Chinese) DOI：10.19789/j.1004-9398.2023.02.009.

Zhang S , Li B, Wang XH, et al. 2021. Study on solute transport in Vadose zone based on Hydrus-1D model. Arid Environmental Monitoring, 3: 97−102. (in Chinese) DOI：10.3969/j.issn.1007-1504.2021.03.001.

Zhang WJ , Wang NA, Yu XR, et al. 2020. Magnitude of groundwater evapotranspiration in the Badain Jaran Desert based on groundwater dynamics method and empirical model: A case study of the Sumujilin Lake Area. Arid Zone Research, 37(5): 1215−1222. (in Chinese) DOI：10.13866/j.azr.2020.05.14.

Zhang XY, Fan XL, Tian MZ. 2022. Mineralogical characteristics and its significance of late Pleistocene sediments in the Badain Jaran Desert. Arid Land Georgraphy, 6: 1773−1783. (in Chinese) DOI：10.12118/j.issn.1000-6060.2022.051.

Zhang YF, Ma YJ, Su ZZ, et al. 2022. Dune movement in the joint zone of the Badain Jaran

Desert and Tengger Desert. Journal of Desert Research, 5: 82−91. (in Chinese) DOI：10.7522/j.issn.1000-694X.2022.00020.

Zhong XJ , Gao YX, Ma K, et al. 2016. Analysis of rainfall variation in Hinterland of Taklamakan Desert. Bulletin of Soil and Water Conservation, 6: 303−307. (in Chinese) DOI：10.13961/j.cnki.stbcxb.2016.06.051.